Multifunctional Analytical Platform on a Paper Strip: Separation, Pre-concentration and Sub-Attomolar Detection.

ARTICLE *in* ANALYTICAL CHEMISTRY · FEBRUARY 2013

Impact Factor: 5.64 · DOI: 10.1021/ac303567g · Source: PubMed

6 AUTHORS, INCLUDING:

Andrew Brimer
Washington University in St. Louis
2 PUBLICATIONS **36** CITATIONS
SEE PROFILE

Limei Tian
University of Illinois, Urbana-Champaign
40 PUBLICATIONS **560** CITATIONS
SEE PROFILE

Srikanth Singamaneni
Washington University in St. Louis
140 PUBLICATIONS **2,760** CITATIONS
SEE PROFILE

analytical chemistry

Article

pubs.acs.org/ac

Multifunctional Analytical Platform on a Paper Strip: Separation, Preconcentration, and Subattomolar Detection

Abdennour Abbas,[†] Andrew Brimer,[†] Joseph M. Slocik,[‡] Limei Tian,[†] Rajesh R. Naik,[‡] and Srikanth Singamaneni*,[†]

[†]Department of Mechanical Engineering and Materials Science, Washington University in St. Louis, St. Louis, Missouri 63130, United States

[‡]Soft Matter Materials Branch, Materials and Manufacturing Directorate, Wright Patterson Air Force Base, Dayton, Ohio 45433, United States

Supporting Information

ABSTRACT: We report a plasmonic paper-based analytical platform with functional versatility and subattomolar ($<10^{-18}$ M) detection limit using surface-enhanced Raman scattering as a transduction method. The microfluidic paper-based analytical device (μPAD) is made with a lithography-free process by a simple cut and drop method. Complex samples are separated by a surface chemical gradient created by differential polyelectrolyte coating of the paper. The μPAD with a starlike shape is designed to enable liquid handling by lateral flow without microchannel patterning. This design generates a rapid capillary-driven flow capable of dragging liquid samples as well as gold nanorods into a single cellulose microfiber, thereby providing an extremely preconcentrated and optically active detection spot.

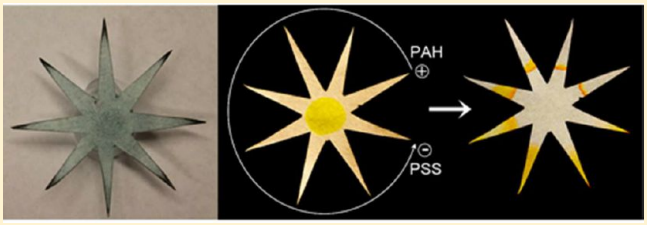

Paper is a versatile and common material that finds many uses in consumer-oriented products because its source (cellulose) is abundant in nature, is renewable, and is inexpensively produced and recycled.[1] Paper is also biodegradable and biocompatible and has the ability to easily wick and absorb fluids.[2] Paper has gained much interest in recent years as a low-cost and ideal platform for building portable miniature diagnostic devices suitable for developing countries, resource-limited environments, and point-of-care settings.[3,4] Paper-based chemical and biological sensing has emerged as an attractive analytical and detection platform with a potential of becoming the best trade-off among cost/time efficiency, simplicity, and detection abilities. The detection is traditionally performed by fluorescence, chemiluminescence, or electrochemical sensing,[5−7] and mostly directed toward labeling methods using antibodies or colorogenic reactions.[8,9] The past few years have witnessed the integration of microfluidic paper-based analytical devices (μPADs) with electrically or optically active nanomaterials such as carbon nanotubes[8] and graphene.[10]

We and others have recently introduced a highly sensitive paper-based surface-enhanced Raman scattering (SERS) substrate which involves uniform adsorption of metal nanostructures onto common filter paper.[11−14] SERS enables label-free detection of a wide variety of chemical and biological analytes. However, current paper-based SERS substrates lack key functionalities such as separation, chemical selectivity, and preconcentration, which are critical to realize a versatile lab-on-chip platform. In other words, for these sensors to be able to analyze complex samples, separation abilities need to be integrated into the paper. While increasing efforts have been focused on extending functionality of the paper substrate,[5,15−19] these developments usually involve lithographic processes or multilayer fabrication,[18,20−22] which is achieved at the expense of the simplicity of the paper device.

The challenge is then to design and develop a highly sensitive label-free analytical platform that does not require any lithographic or microfabrication steps, while providing a multifunctional platform. The second challenge addressed in this work is to significantly lower the detection limit beyond the nanomolar or part per billion (ppb) level reported in recent literature for different μPAD configurations (Table S1, Supporting Information).[4−7,23−27] We seek a versatile system that allows separation and preconcentration of the different components of a complex sample in a small surface area and a label-free optical detection by taking advantage of the properties of cellulose paper: the capillary effect that is attracting increasing interest among the lab-on-a-chip community,[3,12,16,28] the microfibrous structure and the suitability for nanoparticle adsorption by a simple immersion or drop-casting.

EXPERIMENTAL SECTION

Reagents and Materials. The chemicals rhodamine 6G (R6G), fluorescein isothiocyanate (FITC), 2-naphtalenethiol,

Received: December 9, 2012
Accepted: February 20, 2013

   dx.doi.org/10.1021/ac303567g | Anal. Chem. XXXX, XXX, XXX−XXX

poly(allylamine hydrochloride) (PAH), and poly(sodium 4-styrenesulfonate) (PSS) were all obtained from Sigma-Aldrich (St. Louis, MO). PAH (2%) and PSS (2%) solutions were prepared by dissolving 20 mg of PAH or PSS powder in 1 mL of deionized water. These solutions were diluted to prepare 1%, 0.5%, and 0.25% polyelectrolyte solutions. The chlorophyll mixture was obtained by the extraction of spinach concentrate.

Gold nanorods (AuNRs) were synthesized using a seed-mediated approach.[29,30] The seed solution was prepared by adding 0.6 mL of an ice-cold solution of 10 mM sodium borohydride to 10 mL of 0.1 M cetyltrimethylammonium bromide (CTAB) and 2.5×10^{-4} M $HAuCl_4$ solution under magnetic stirring at room temperature. The color of the solution changed from yellow to brown. Growth solution was prepared by mixing 95 mL of 0.1 M CTAB, 1.25 mL of 10 mM silver nitrate, 5 mL of 10 mM $HAuCl_4$, and 0.55 mL of 0.1 M ascorbic acid in the same order. The solution was homogenized by gentle stirring. To the resulting colorless solution 0.12 mL of freshly prepared seed solution was added, and the resulting solution was set aside in the dark for 14 h. The solution turned from colorless to green, with most of the color change happening within the first hour. Prior to use, the AuNR solution was centrifuged twice at 13 000 rpm for 10 min to remove excess CTAB and then redispersed in nanopure water. The synthesized nanorods have an average size of 20 nm × 60 nm (Figure 1A).

Surface and Materials Characterization. SERS spectra were collected using a Renishaw inVia confocal Raman spectrometer mounted on a Leica microscope with a 50× objective (NA = 0.90) in the range of 100−3200 cm^{-1}. A diode laser of 785 nm wavelength (0.5 mW) was used for sample excitation. Optical and fluorescence images of the μPAD were obtained with a Leica optical microscope (DM 4000M) coupled with a point-shot microspectrometer using 20× and 50× objectives. Fluorescence spectra were obtained from paper substrates using a CRAIC microspectrophotometer (QDI 302) coupled to the above-mentioned optical microscope. Transmission electron microscopy (TEM) images and energy-dispersive X-ray spectroscopy (EDX) maps were obtained using a field emission transmission electron microscope (JEM-2100F, JEOL) operating at an accelerating voltage of 200 kV, and scanning electron microscopy (SEM) images were collected using a JEOL JSM-7001 FLV field emission scanning electron microscope at an accelerating voltage of 15 kV. Elementary analysis (atomic ratio) of the carbon, nitrogen (N1s), and sulfur (S2p) composition of the paper was achieved by X-ray photoelectron spectroscopy (XPS) using an M-Probe Surface Science XPS spectrometer.

RESULTS AND DISCUSSION

Filter paper employed in this study (Whatman no. 1) is composed of microscale (~10 μm) cellulose fibrous strands interwoven together. Smaller microfibers (average diameter of ~0.4 μm) made part of the large fibrous structure with nanofibers braided in between. The RMS surface roughness of the paper was measured to be ~70 nm over a 5×5 μm^2 area, indicating that the paper offers a large surface area. To keep the device fabrication process simple, the filter paper was cut into a starlike geometry with eight points named fingers (Figure 1B). This design obviates the need for lithographic or hydrophobic patterning of the paper while offering an effective liquid handling system using capillary forces. The shape-enhanced capillary forces, i.e., the small size of the tips (the radius of the tips is ~10−20 μm), result in a much faster drying of the solvent at the tips compared to the rest of the paper substrate, in turn causing a rapid flow from the wetted surface to the dry area, thus concentrating the analytes to the tiny test regions. Interestingly, these strong capillary effects make the flow strong enough to drag not only macromolecules but also gold nanorods with a length of ~60 nm.

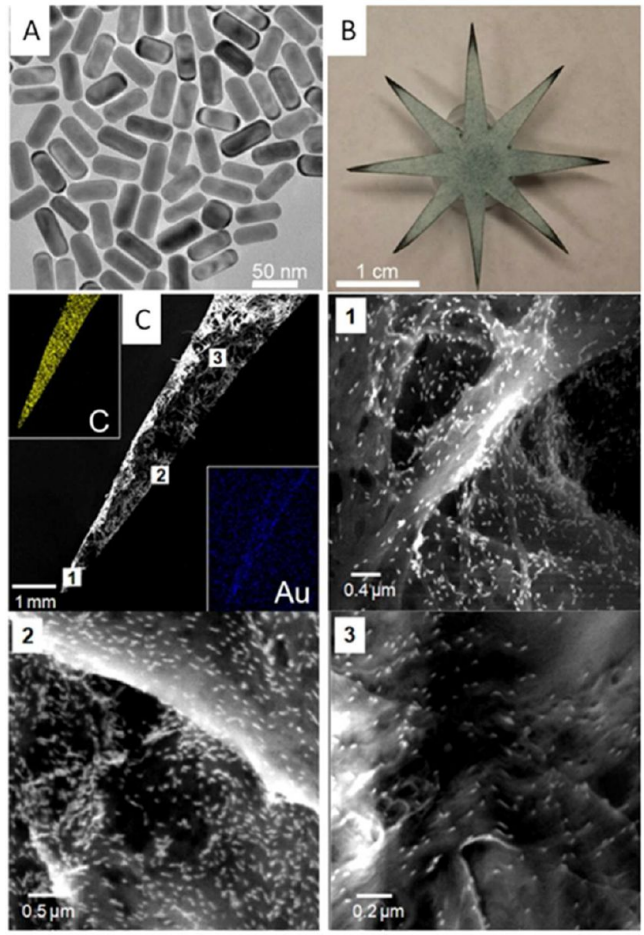

Figure 1. (A) TEM image of the AuNRs employed for the fabrication of SERS μPAD. (B) Designed μPAD with eight fingers showing the accumulation of AuNRs at the tips (dark edges). (C) SEM images of the μPAD tips. The insets represent EDX maps of carbon and gold distribution. A zoom at the fingertip shows the nanorod distribution at three different spots labeled 1, 2, and 3 as a result of lateral flow concentration.

AuNRs were employed as plasmonic nanostructures for enabling SERS owing to the facile tunability of the longitudinal plasmon resonance (to fit to the source laser) and sharp corners, which results in electromagnetic hot spots (Figure 1A).[31,32] Figure 1B shows that immersion of the paper into AuNR solution results in a preferential concentration of the nanorods at the fingertips and edges of the device. Even simple visual inspection clearly indicates such concentration of AuNRs at the tips, which appear darker compared to the other regions of the paper (Figure 1B). SEM images and EDX maps obtained from different regions of the paper substrates clearly demonstrate this effect (Figure 1C). This is of great importance as the accumulation of the nanorods in a small area increases the number of electromagnetic hot spots, thus enhancing the sensitivity of the optical detection.[33−35] This enhancement is exploited here using SERS as the transduction method.[25,36]

dx.doi.org/10.1021/ac303567g | Anal. Chem. XXXX, XXX, XXX−XXX

In addition to AuNR transport, the capillary-driven flow is also used here to drag and preconcentrate samples at the μPAD tips, thus providing enough analyte in the test spot for detection even at very low sample concentrations. To enable analyte preconcentration on paper and at the same time separate complex samples, we explored the possibility of using polyelectrolytes. Each finger of the μPAD was modified with a different concentration of PAH (positively charged) or PSS (negatively charged) (Figure 2A). This modification is achieved

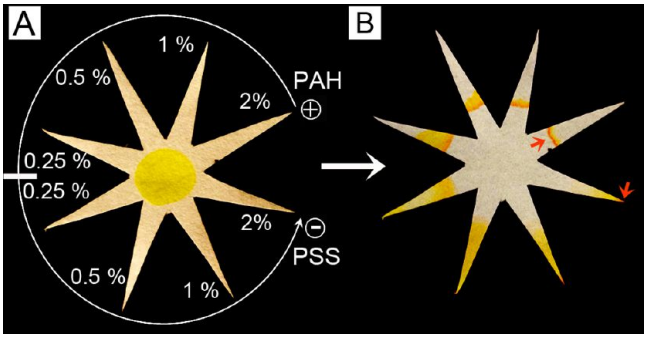

Figure 2. Separation by surface charge gradient. (A) Charge gradient obtained by different concentrations of PAH and PSS polyelectrolytes. The yellow spot at the center is caused by a fluorescein droplet as deposited. (B) Migration of fluorescein into different fingers. The red arrows indicate the concentration at which fluorescein forms either a band or concentrates at the tip.

by exposing the tip of each finger to a droplet of polyelectrolyte solution (3 μL) with a defined concentration as indicated in Figure 2A. The droplet is spontaneously absorbed by the paper and rapidly spread along a single finger without reaching other areas of the platform. As a result, the different polyelectrolyte-coated fingers form a gradient of charges that control the direction and distance of migration of the analytes, depending on their electrostatic interactions with the charged substrate. We hypothesize that complex samples could be separated and directed into different fingers of the μPAD. The chemical surface gradient formed by the differential functionalization of the fingers is confirmed by EDX mapping. The distribution of the polyelectrolytes is monitored by the detection of nitrogen and sulfur atoms in PAH and PSS, respectively (Figure 3). The elemental analysis by XPS also confirmed the decrease in S2p and N1s atomic composition, reflecting the different concentrations of PSS and PAH on different fingers.

The first example demonstrating the effect of the chemical gradient is shown in Figure 2B using fluorescein. Depending on the charge and concentration of the polyelectrolyte coating, fluorescein forms a distinct band or completely migrates to the fingertip. Specifically, we observed that fluorescein tends to concentrate at the fingertip coated with 2% PSS. On the other hand, it forms a distinct band at the entrance of the finger coated with 2% PAH. Considering that fluorescein is negatively charged in water, it tends to strongly bind to the positively charged PAH, resisting any capillary-driven motion to the tips. On the other hand, in the case of the PSS-coated fingers, the capillary forces drag the fluorescein along the finger and concentrate them at the tips. This observation clearly hints that potentially different molecules (i) can migrate into different fingers, which provides the most electrostatically compatible surface, and (ii) can be concentrated at the tip, thus providing an extremely high concentration in a very small surface area. To further demonstrate the separation ability of this platform, we have analyzed a mixture of rhodamine and fluorescein.

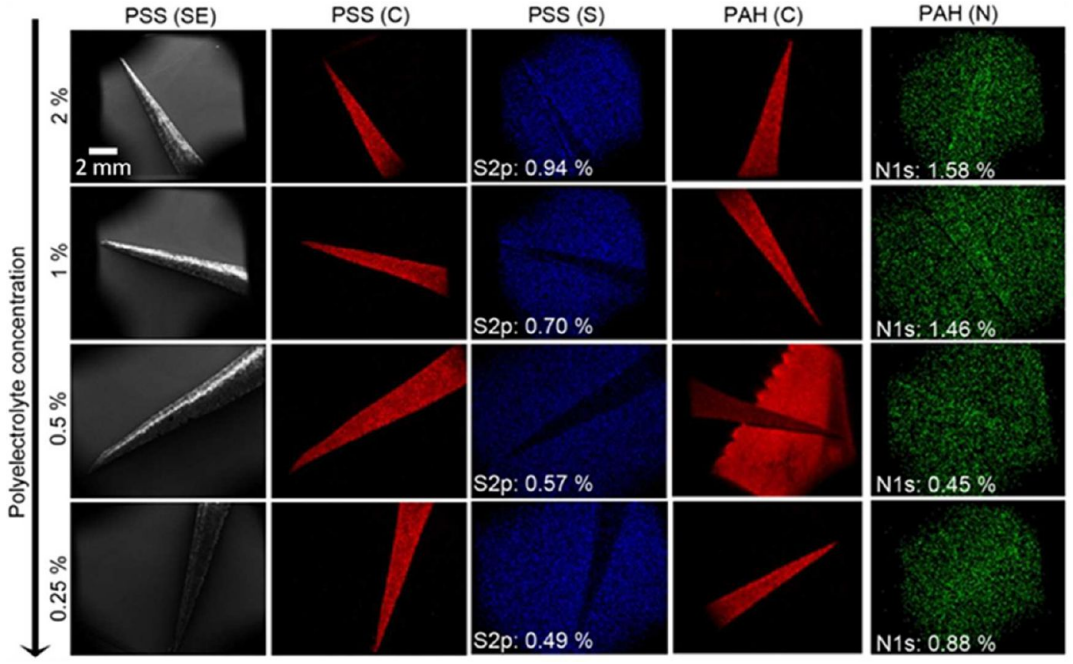

Figure 3. EDX mapping and XPS elementary analysis of the surface charge gradient generated by differential polyelectrolyte coating. The panel "PSS (SE)" represents secondary electron (SE)-SEM micrographs of the μPAD fingers coated with PSS. Panels "PPS (C)" and "PAH (C)" represent EDX mapping of carbon atoms on PSS- and PAH-coated fingers, respectively. These two panels are shown to indicate the position of the fingers in the images and facilitate comparison. Panels "PSS (S)" and "PAH (N)" represent EDX mapping of sulfur and nitrogen atoms in PSS- and PAH-coated fingers, respectively. The percentage numbers indicated in the images represent the composition ratio of sulfur (S2p) and nitrogen (N1s) obtained by XPS elementary analysis.

dx.doi.org/10.1021/ac303567g | Anal. Chem. XXXX, XXX, XXX−XXX

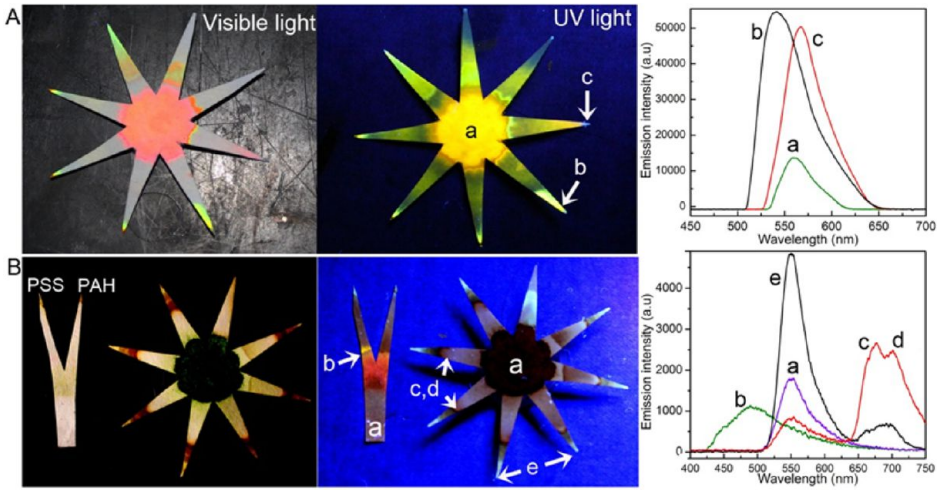

Figure 4. Separation of complex samples by an electrostatic gradient charge and capillary forces. Images from the left to the right show the μPAD under visible light and under UV light and the emission spectra obtained using a fluorescence microscope. (A) Separation of (a) a mixture of two molecular dyes. (b) and (c) are respectively fluorescein and R6G dyes. (B) Separation of spinach concentrate (a). The lowercase letters (b–e) in panel B represent respectively carotene, xanthophyll, chlorophyll *a*, and chlorophyll *b*.

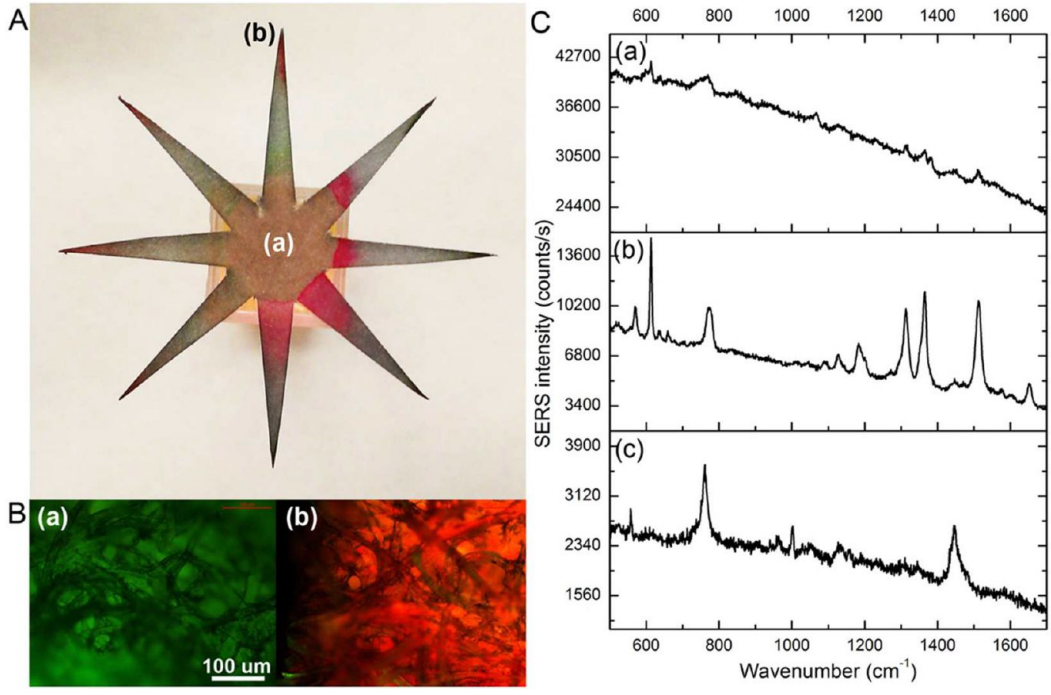

Figure 5. Separation and SERS detection of R6G in a mixture containing spinach concentrate. (A) Optical image of the paper platform at the end of the separation step. (B) Fluorescence images obtained with an I3 filter at the center and fingertip of the platform. (C) Surface-enhanced Raman scattering analysis. (a) and (b) refer respectively to data collected at the center and at the fingertip of the platform. (c) shows the SERS spectrum of a control (nanorod-functionalized paper).

Rhodamine is known to bear a positive charge, while fluorescein is known to be negatively charged in water. Distinct electrostatic interaction with different fingers enables spatially isolating the two dyes on the μPAD as demonstrated in Figure 4A. Furthermore, using a similar principle, a more complex sample composed of chlorophyll *a*, chlorophyll *b*, carotene, and xanthophyll, obtained from spinach concentrate, can also be separated using such differential functionalization of the paper substrates (Figure 4B). The identification of the different separated components is confirmed by their emission spectra under a fluorescence microscope.

A more complex matrix was prepared by mixing 100 μM R6G with a one-time diluted spinach concentrate. This sample is used to demonstrate two important points: The first is that the μPAD is able to separate and preconcentrate R6G molecules from the other chromophores contained in the spinach concentrate as shown in Figure 5A,B. The distribution of R6G demonstrates a preferential concentration at the fingertips functionalized with PAH. Second, one of the components of spinach concentrate (chlorophyll *b*) exhibits fluorescence emission in the same wavelength range as R6G. As a result fluorescence spectroscopy is not sufficient to clearly distinguish between these two components. Figure 5B shows

dx.doi.org/10.1021/ac303567g | *Anal. Chem.* XXXX, XXX, XXX–XXX

that SERS spectroscopy enables one to specifically identify R6G molecules, thus demonstrating the productive complementarity of SERS and fluorescence techniques and the advantages provided by plasmonic paper platforms.

Once we have established the ability to separate and preconcentrate the analytes from a complex mixture to predetermined locations of the μPAD, we turn our attention to trace detection capabilities of this novel analytical platform. To evaluate the detection limit of the μPAD and the advantages offered by the capillarity-driven preconcentration at the fingertips, we attempt to detect different concentrations of R6G (Figure 6A). The results indicate a remarkable detection

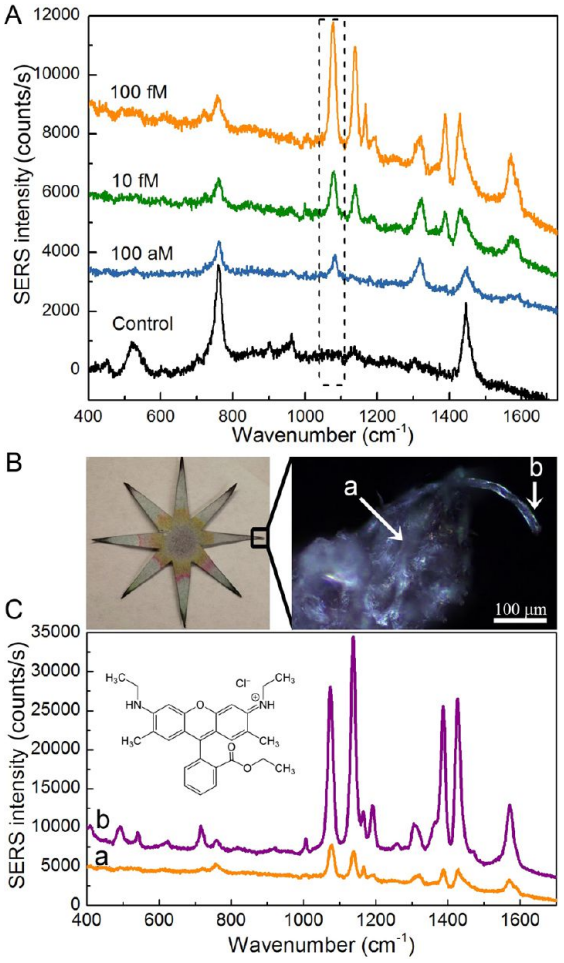

Figure 6. Surface-enhanced Raman scattering analysis of R6G (λ = 785 nm). (A) Detection of different concentrations of R6G. (B) Optical image of the μPAD. The zoom shows a dark field image of the tip, where (a) and (b) show the position of the laser spot used to collect the R6G spectra shown in (C).

limit down to the attomolar level (100 aM). This limit can be further lowered by concentrating the analyte in a micrometric surface area, corresponding to a single cellulose microfiber at the very tip of the finger (Figure 6B; Figure S1a, Supporting Information). The preconcentration factor can be estimated from the paper properties, the initial concentration, and data obtained by SERS measurement. The concentration of 100 aM in 100 μL of sample corresponds to around 6×10^6 molecules. As indicated by fluorescence images, most of these molecules can be preconcentrated at the paper fingertip into a surface area smaller than 1 mm^2 (the paper thickness is 180 μm). Knowing that the filter paper (Whatman no. 1) has a water absorbance of 1.8 ± 0.2 $\mu L/cm^2$ as determined experimentally, the final sample concentration at the fingertip is estimated to be 0.5 nM, which gives a remarkable preconcentration factor of 10^9. This factor can be further enhanced by working with a single cellulose microfiber where the sample can be concentrated into an extremely tiny volume, i.e., fiber of 50 μm length (Figure S1b). Figure 6C shows the increase in the SERS intensity when the Raman laser spot is focused onto the fingertip region labeled "b". The SERS measurement on the microfiber tip provides an additional 10× improvement in the detection limit.

To further verify this result, we prepared paper substrates with tips ending with a single cellulose microfiber of around 20 μm in diameter. Two different analytes, namely, fluorescein and napthalenethiol, were tested. The test domains exhibited a detection limit of ∼100 aM for fluorescein, while no characteristic band was observed when the detection was performed outside the microfiber (Figure 7A,B). Even better performance was noted for naphtalenethiol (due to its strong affinity for gold), which showed a remarkable detection limit of 500 zM (signal-to-noise ratio (SNR) equal to 3). This detection limit is also the result of the thiol binding of the molecule to AuNRs, offering an optimal distance for SERS. However, this performance has a very limited dynamic range going from 500 zM to 10 μM. This is expected as higher concentrations rapidly saturate the micrometric detection spot. To verify the applicability of this platform on a real world sample, 2-naphtalenethiol (1 μM) was added to tap water and the obtained solution introduced to the paper platform for separation and detection. Interestingly, Figure S2A (Supporting Information) shows a visible separation and accumulation of the different water ions (K, Na, Ca, Mg, Cl, ...) at the paper fingers functionalized with PSS. This unexpected accumulation makes the migration of the target molecules in other fingers easier by reducing the molecular crowding. As depicted in Figure 2SB, the platform can be effectively used to detect 2-naphtalenethiol and other aromatic contaminants in tap water.

The studies reported here with R6G and FTIC represent the lowest detection limit reported for μPADs. It is interesting to note that this performance is only limited by the size of the laser spot in the Raman instrument and the available sample volume. In other words, a concentration of 100 zM (10^{-19} M) corresponds to only six molecules in the test solution volume (100 μL). Therefore, beyond the attomolar level, higher sample volume is needed to ensure the presence of the molecule in the detection spot. Future efforts are aimed to shorten the migration time of the molecule to the detection spot and improve the separation abilities by exploring a variety of polymers as well as silica nanoparticles for a column-chromatography-like separation.

CONCLUSIONS

In summary, we demonstrate a plasmonic paper-based analytical platform that combines chromatographic separation abilities with preconcentration and detection functionalities in a single-level μPAD. The use of capillary forces by shaping the paper substrate overcomes the need for active microfluidics and the associated microfabrication process. The generation of a charge gradient on the paper substrate through polyelectrolyte coating is shown to exhibit remarkable separation abilities of complex samples. The results also show that capillary-driven flow could be used for the transport and preconcentration of both analytes and metal nanoparticles in a very small detection

dx.doi.org/10.1021/ac303567g | Anal. Chem. XXXX, XXX, XXX−XXX

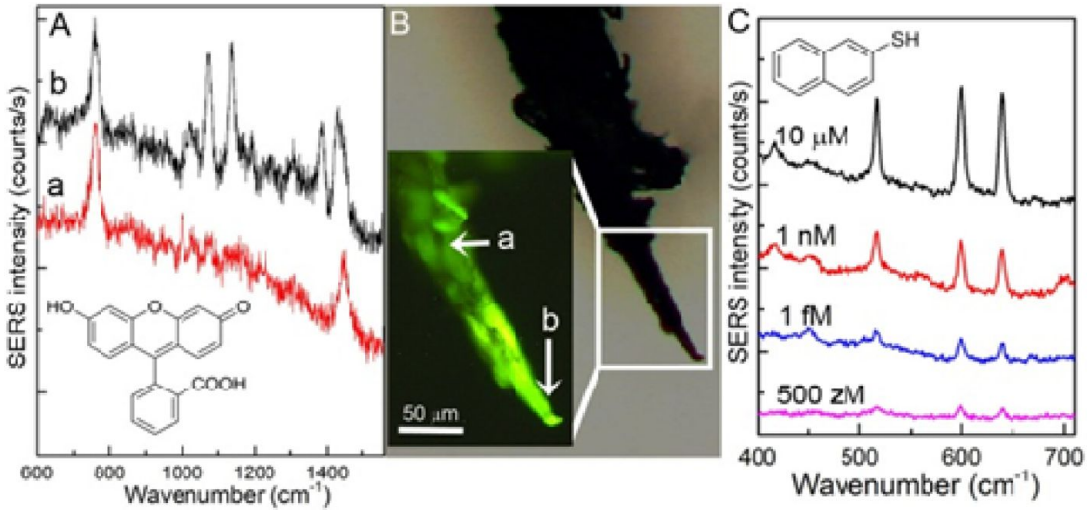

Figure 7. SERS detection limit on a single cellulose microfiber. (A) Detection of 100 aM fluorescein. (a) and (b) represent SERS spectra collected at the positions indicated in (B). The bands at 1075, 1138, and 1385 cm^{-1} are assigned to fluorescein. (B) Optical and fluorescence images of the μPAD tip. (C) Detection of 2-naphthalenethiol. The peaks at 516, 600, and 638 cm^{-1} are assigned to ring deformation and twisting.

area and even on a single cellulose microfiber. The combination of this concept with surface-enhanced Raman scattering analysis pushes the detection limit down to the attomolar level, placing microfluidic paper-based analytical devices in a competitive stand with the traditional sensors and without scarifying their simplicity.

■ ASSOCIATED CONTENT

Ⓢ Supporting Information

Additional information as noted in text. This material is available free of charge via the Internet at http://pubs.acs.org.

■ AUTHOR INFORMATION

Corresponding Author

*E-mail: singamaneni@wustl.edu.

Notes

The authors declare no competing financial interest.

■ ACKNOWLEDGMENTS

This work was supported by the Materials and Manufacturing Directorate, Air Force Research Laboratory (AFRL/RX).

■ REFERENCES

(1) Samir, M. A. S. A.; Alloin, F.; Dufresne, A. *Biomacromolecules* **2005**, *6*, 612.
(2) Martinez, A. W.; Phillips, S. T.; Whitesides, G. M.; Carrilho, E. *Anal. Chem.* **2010**, *82*, 3.
(3) Martinez, A. W.; Phillips, S. T.; Carrilho, E.; Thomas, S. W.; Sindi, H.; Whitesides, G. M. *Anal. Chem.* **2008**, *80*, 3699.
(4) Ellerbee, A. K.; Phillips, S. T.; Siegel, A. C.; Mirica, K. A.; Martinez, A. W.; Striehl, P.; Jain, N.; Prentiss, M.; Whitesides, G. M. *Anal. Chem.* **2009**, *81*, 8447.
(5) Nie, Z.; Nijhuis, C. A.; Gong, J.; Chen, X.; Kumachev, A.; Martinez, A. W.; Narovlyansky, M.; Whitesides, G. M. *Lab Chip* **2010**, *10*, 477.
(6) Ge, S.; Ge, L.; Yan, M.; Song, X.; Yu, J.; Huang, J. *Chem. Commun.* **2012**, *48*, 9397.
(7) Godino, N.; Gorkin, R.; Bourke, K.; Ducree, J. *Lab Chip* **2012**, *12*, 3281.
(8) Wang, L.; Chen, W.; Xu, D.; Shim, B. S.; Zhu, Y.; Sun, F.; Liu, L.; Peng, C.; Jin, Z.; Xu, C.; Kotov, N. A. *Nano Lett.* **2009**, *9*, 4147.
(9) Ge, L.; Wang, S.; Song, X.; Ge, S.; Yu, J. *Lab Chip* **2012**, *12*, 3150.
(10) Xiao, F.; Li, Y.; Zan, X.; Liao, K.; Xu, R.; Duan, H. *Adv. Funct. Mater.* **2012**, *22*, 2487.
(11) Yu, W. W.; White, I. M. *Anal. Chem.* **2010**, *82*, 9626.
(12) Lee, C. H.; Tian, L.; Singamaneni, S. *ACS Appl. Mater. Interfaces* **2010**, *2*, 3429.
(13) Yu, W. W.; White, I. M. *Analyst* **2013**, *138*, 1020.
(14) Lee, C. H.; Hankus, M. E.; Tian, L.; Pellegrino, P. M.; Singamaneni, S. *Anal. Chem.* **2011**, *83*, 8953.
(15) Lutz, B. R.; Trinh, P.; Ball, C.; Fu, E.; Yager, P. *Lab Chip* **2011**, *11*, 4274.
(16) Osborn, J. L.; Lutz, B.; Fu, E.; Kauffman, P.; Stevens, D. Y.; Yager, P. *Lab Chip* **2010**, *10*, 2659.
(17) Fu, E.; Lutz, B.; Kauffman, P.; Yager, P. *Lab Chip* **2010**, *10*, 918.
(18) Songjaroen, T.; Dungchai, W.; Chailapakul, O.; Henry, C. S.; Laiwattanapaisal, W. *Lab Chip* **2012**, *12*, 3392.
(19) Tian, L.; Morrissey, J. J.; Kattumenu, R.; Gandra, N.; Kharasch, E. D.; Singamaneni, S. *Anal. Chem.* **2012**, *84*, 9928.
(20) Yu, J.; Ge, L.; Huang, J.; Wang, S.; Ge, S. *Lab Chip* **2011**, *11*, 1286.
(21) Liu, H.; Xiang, Y.; Lu, Y.; Crooks, R. M. *Angew. Chem.* **2012**, *51*, 6925.
(22) Martinez, A. W.; Phillips, S. T.; Butte, M. J.; Whitesides, G. M. *Angew. Chem., Int. Ed.* **2007**, *46*, 1318.
(23) Abe, K.; Suzuki, K.; Citterio, D. *Anal. Chem.* **2008**, *80*, 6928.
(24) Aragay, G.; Monton, H.; Pons, J.; Font-Bardia, M.; Merkoci, A. *J. Mater. Chem.* **2012**, *22*, 5978.
(25) Hossain, S. M. Z.; Brennan, J. D. *Anal. Chem.* **2011**, *83*, 8772.
(26) Jokerst, J. C.; Adkins, J. A.; Bisha, B.; Mentele, M. M.; Goodridge, L. D.; Henry, C. S. *Anal. Chem.* **2012**, *84*, 2900.
(27) Wu, X.; Kuang, H.; Hao, C.; Xing, C.; Wang, L.; Xu, C. *Biosens. Bioelectron.* **2012**, *33*, 309.
(28) Hwang, H.; Kim, S.-H.; Kim, T.-H.; Park, J.-K.; Cho, Y.-K. *Lab Chip* **2011**, *11*, 3404.
(29) Lee, K.-S.; El-Sayed, M. A. *J. Phys. Chem. B* **2005**, *109*, 20331.
(30) Gole, A.; Murphy, C. J. *Langmuir* **2007**, *24*, 266.
(31) Huang, X. H.; Neretina, S.; El-Sayed, M. A. *Adv. Mater.* **2009**, *21*, 4880.
(32) Vigderman, L.; Khanal, B. P.; Zubarev, E. R. *Adv. Mater.* **2012**, *24*, 4811.
(33) Abbas, A.; Tian, L.; Morrissey, J.; Kharasch, E. D.; Singamaneni, S. *Adv. Funct. Mater.* **2013**, DOI: 10.1002/adfm.201202370.
(34) Abbas, A.; Fei, M.; Tian, L.; Singamaneni, S. *Plasmonics* **2013**, DOI: 10.1007/s11468-012-9431-8.
(35) Gandra, N.; Abbas, A.; Tian, L. M.; Singamaneni, S. *Nano Lett.* **2012**, *12*, 2645.

(36) Stiles, P. L.; Dieringer, J. A.; Shah, N. C.; Van Duyne, R. P. *Annu. Rev. Anal. Chem.* **2008**, *1*, 601.

dx.doi.org/10.1021/ac303567g | *Anal. Chem.* XXXX, XXX, XXX−XXX